

Spin wave amplification through superradiance

X. R. Wang,^{1,2,3,*} X. Gong,¹ and K. Y. Jing¹

¹*Physics Department, The Hong Kong University of Science and Technology, Clear Water Bay, Kowloon, Hong Kong*

²*HKUST Shenzhen Research Institute, Shenzhen 518057, China*

³*William Mong Institute of Nano Science and Technology,*

The Hong Kong University of Science and Technology, Clear Water Bay, Kowloon, Hong Kong, China

(Dated: August 3, 2023)

Superradiance is a phenomenon of multiple facets that occurs in classical and quantum physics under extreme conditions. Here we present its manifestation in spin waves under an easily realized condition. We show that an interface between a current-free (normal) ferromagnetic (FM) region and a current-flow (pumped) FM region can be a spin wave super-mirror whose reflection coefficient is larger than 1. The super-reflection is the consequence of current-induced spectrum inversion where phase and group velocities of spin waves are in the opposite directions. An incident spin wave activates a backward propagating refractive wave inside pumped FM region. The refractive spin wave re-enters the normal FM region to constructively interfere with the reflective wave. It appears that the pumped FM region coherently emits reflective waves, leading to a super-reflection. The process resembles superradiance of a spinning black hole through the Hawking radiation process, or Dicke superradiance of cavity photons inside population inverted media.

Spin waves have attracted much attention in spintronics due to their rich physics [1–3] and potential applications [4–7]. One challenge in spin-wave based applications is the strong spin wave damping such that it can only propagate a relatively short distance, order of millimetres even for yttrium iron garnets [8, 9] with the lowest damping coefficient. Thus, an effective method for amplifying an arbitrary spin wave is demanded in order to realize the power of spin waves.

Many efforts have been made on spin wave amplification. The anti-damping nature of spin transfer torques (STTs) [10–13] and spin orbit torques [14–16] was considered first. The Landau-Lifshitz-Gilbert (LLG) equation suggests that spin torques can exponentially amplify all spin waves [11]. Unfortunately, experiments and micromagnetic simulations observed only the increase of spin wave propagation distance, but no spin wave amplification [10–16] with probably one exception [17]. Parametric pumping has also been used to amplify spin waves. The idea is to resonate spin waves with external oscillating fields such as an electromagnetic or a mechanic wave [18–23]. At resonance, energy from external fields can be transformed into the energy of a spin wave. However, parametric pumping requires specific resonant conditions that are only applicable to a particular wave frequency. The Klein paradox [24, 25] has been proposed to amplify spin waves. The concept involves using STTs or spin-orbit torques to create a spin wave analogue of black and white holes [26, 27] such that positive-energy and negative-energy spin wave modes can be coupled together in an inhomogeneous FM film. Experimental realization of this proposal is yet to be done. Nonlinear 3-magnon and 4-magnon process have also been proposed to amplify spin waves and to create spin wave combs [28]. This approach often requires stringent conditions and for a specific mode.

Reflection and refraction are general wave phenomena occurring at an interface between two homogeneous media. A general rule is that intensities of both reflective and refractive waves are smaller than that of the incoming wave due to the energy conservation law. The frequency (energy) minimum of wave spectrum in a normal media is at zero wave number such that the group and phase velocities are in the same directions (for isotropic media). An adiabatic spin-transfer torque from an electric current along the spin wave propagating direction can invert the spin wave spectrum in which the group and phase velocities in certain frequency window could be in the opposite directions. Such a current-flow region is termed a pumped medium. In an electric-current-flow magnetic film, spin wave spectrum is inverted along the current direction. Surprisingly and interestingly, the reflection coefficient of a wave at the interface between a normal medium and a pumped medium can be greater than 1. It appears that pumped region is coherently emitting spin waves to the normal region. The process resembles superradiance [25] of a spinning black hole through the Hawking radiation, or the Dicke superradiance of cavity photons inside population inverted media.

In this letter, we show that an interface between a current-free and a current-flow FM regions can be super-mirror for spin wave in a frequency range tunable by an electric current. A wave packet in the pumped medium propagates forward (positive group velocity) while waves of given negative wave numbers move backward (negative phase velocities) to emit backward spin waves at the interface. The emitted waves interfere constructively with the reflective waves, leading to the super-reflection. The physics is clearly revealed in a generic FM model and is confirmed by micromagnetic simulations.

We consider a thin magnetic film of thickness d laying in the xy -plane as shown in Fig. 1. The film on the

left ($x < 0$) is current-free and film on the right ($x > 0$) has an electric current density \vec{j} flowing along the x -direction (\hat{x}) such that the spin wave spectrum minimum is at wave vector $\vec{k} = (k_0, 0)$ ($k_0 \propto j < 0$). The middle panel of Fig. 1 illustrates an incident wave of ω and \vec{k}_1 , and reflective wave of ω and \vec{k}'_1 and refractive wave of ω and \vec{k}_2 . The left and right panels are the schematic plots of normal and inverted spin wave spectrum along $\vec{k} = (k, 0)$, respectively. ω is minimum at $k_0 \neq 0$ in the inverted spectrum and phase and group velocities are opposite in sign for $\omega \in [\omega_{\min}, \omega_{\max}]$. Magnetization state $\vec{M}(\vec{x}, t) = M_s \vec{m}(\vec{x}, t)$ with saturation magnetization M_s and direction \vec{m} is described by the magnetic energy,

$$E = d \int [A(\nabla \vec{m})^2 + K_u(1 - m_z^2) - \frac{1}{2} \mu_0 M_s \vec{H}_d \cdot \vec{m}] dx dy, \quad (1)$$

where A , K_u , \vec{H}_d and μ_0 are the exchange stiffness constant, the crystalline magnetic anisotropy, the demagnetizing field and the vacuum permeability, respectively. The demagnetization effect can be included in the effective anisotropy $K = K_u - \mu_0 M_s^2/2$ for an ultra-thin film [29]. Her we mimic Co/Pt film with $M_s = 0.6 \text{ MA m}^{-1}$, $A = 10 \text{ pJ m}^{-1}$, $K_1 = 0.6 \text{ MA m}^{-3}$ in normal region and $K_2 = 0.9 \text{ MA m}^{-3}$ in the inverted region. Magnetization dynamics is governed by the LLG equation,

$$\frac{\partial \vec{m}}{\partial t} = -\gamma \vec{m} \times \vec{H}_{\text{eff}} + \alpha \vec{m} \times \frac{\partial \vec{m}}{\partial t} - (\vec{u} \cdot \nabla) \vec{m}, \quad (2)$$

where γ and α are respectively the gyromagnetic ratio and the Gilbert damping constant. $\alpha = 0.001 \sim 0.005$ is used in this study. The effective field is $\vec{H}_{\text{eff}} = -(\mu_0 M_s)^{-1} \delta E / \delta \vec{m}$. $\vec{u} = \frac{P \mu_B}{e M_s} \vec{j}$ is the spin drift velocity, here P , μ_B , $e (> 0)$, and \vec{j} are the spin polarization, the Bohr magneton, electron charge, and the applied current density, respectively. $\vec{j} = 10^{13} \hat{x} \text{ A m}^{-2}$ [30, 31] in the inverted medium is used throughout this study with spin polarization $P = 1$ if not stated otherwise. Although only an adiabatic STT is included here, including a non-adiabatic STT will not change physics, see evidences and discussions in Supplemental Material.

Eq. (2) is numerically solved by MuMax3 [32], and spin wave spectrum is obtained by the Fourier analysis of thermally generated random $\vec{m}(\vec{x}, t)$ directly from MuMax3 (see Supplemental Material for details). To investigate spin wave reflection and refraction, we simulate Eq. (2) with an oscillating magnetic field along a narrow strip at lower left corner of the film, the black bar in Fig. 1. To avoid boundary effects, we add absorb regions at boundaries with a large Gilbert damping $\alpha = 0.5$.

Without STTs, the LLG equation describes dissipative dynamics [33] if $\alpha \neq 0$ and the system ends at a ferromagnetic state, $\vec{m} = \pm \hat{z}$. The LLG equation is a Hamiltonian system if $\alpha = 0$ and the system shall move on equal-energy contours [33]. In the presence of STT and with a damping, $\vec{m} = \pm \hat{z}$ are stable against STT

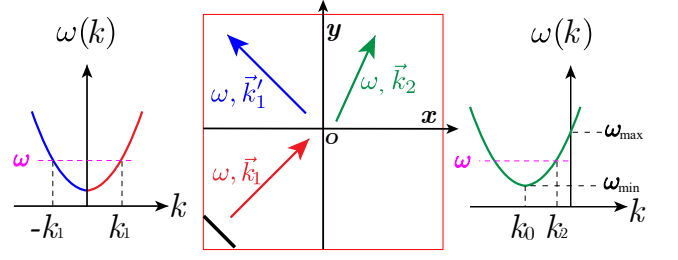


FIG. 1. Schematic illustration of a incident spin wave of frequency ω and wave vector of \vec{k}_1 , reflective wave of ω and \vec{k}'_1 , and refractive wave of ω and \vec{k}_2 . The black bar donates spin wave source from an oscillating magnetic field. The normal and inverted spectra are schematically illustrated in the left and right panels, respectively.

agitations due to the quick damping of spontaneously generated spin waves. Without a damping and with a STT, the STT can do work in an inhomogeneous region (inevitably near sample boundary and around defects in reality) and generates all types of spin waves such that no static state is possible as shown by the blue curve in Fig. 2(a). Spin waves are the normal modes of small fluctuation of \vec{m} , $\vec{m} = m_x \hat{x} + m_y \hat{y} + \hat{z}$, $m_x, m_y \ll 1$, govern by

$$\begin{pmatrix} \partial_t + \vec{u} \cdot \nabla & -A' \nabla^2 + K' + \alpha \partial_t \\ A' \nabla^2 - K' - \alpha \partial_t & \partial_t + \vec{u} \cdot \nabla \end{pmatrix} \begin{pmatrix} m_x \\ m_y \end{pmatrix} = 0, \quad (3)$$

where $A' = \frac{2\gamma A}{\mu_0 M_s}$, $K' = \frac{2\gamma K}{\mu_0 M_s}$ and $\vec{u} = \frac{P \mu_B}{e M_s} \vec{j}$ (0 for $x < 0$). In terms of $\varphi \equiv m_x + i m_y$, Eq. (3) becomes,

$$-i \frac{\partial \varphi}{\partial t} = \frac{1 + i\alpha}{1 + \alpha^2} (-A' \nabla^2 + K' + i \vec{u} \cdot \nabla) \varphi, \quad (4)$$

with spin wave solutions of $\varphi = \sum_k a_k e^{-\vec{\Lambda} \cdot \vec{r}} e^{i(\omega t - \vec{k} \cdot \vec{r})}$ and spectrum of

$$\omega = A' |\vec{k}|^2 + K' + \vec{u} \cdot \vec{k}. \quad (5)$$

$a_k e^{-\vec{\Lambda} \cdot \vec{r}}$ is the exponential decay of the amplitude. The decay length $|\vec{\Lambda}|^{-1}$ is given by $\vec{\Lambda} \cdot \vec{v} = \alpha \omega$. $\vec{v} = 2A' \vec{k}$ ($2A' \vec{k} + \vec{u}$) is the group velocity in the current-free (current-flow) region. Spin waves are gapped with gap K'_1 in region 1, and $K'_2 - u^2/4A'$ in region 2. Figures 2(c) and (d) show the spectrum of spin waves along $\vec{k} = (k, 0)$, where colors denote density plot and curves are analytic formula Eq. (5) (in terms of linear frequency $f = \omega/2\pi$), which agrees with simulations.

Spin wave satisfies continuity conditions at the interface, $\varphi(x = 0^-) = \varphi(x = 0^+)$ and $\nabla \varphi(x = 0^-) = \nabla \varphi(x = 0^+)$. For a normally incident spin wave of frequency ω , $\varphi(x, t) = B e^{-\Lambda_1 x} e^{i(\omega t - k_1 x)} + C e^{\Lambda_1 x} e^{i(\omega t + k_1 x)}$ for $x < 0$ and $\varphi(x, t) = D e^{-\Lambda_2 x} e^{i(\omega t - k_2 x)}$ for $x > 0$. Reflection coefficient R and transmission coefficient T can

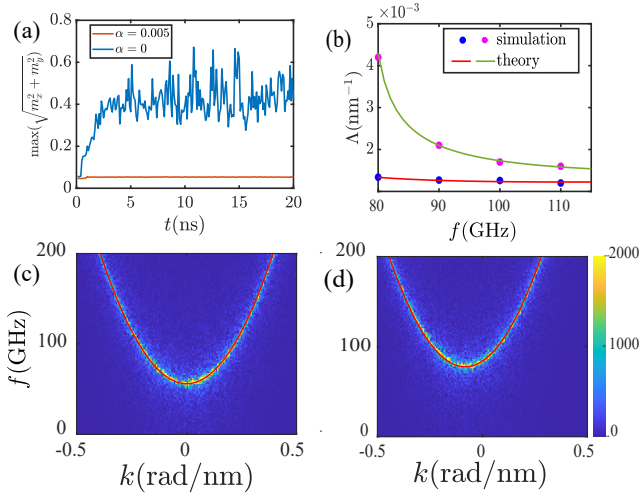


FIG. 2. (a) $\vec{m} = \hat{z}$ under a current is no longer an equilibrium state when $\alpha = 0$ (the blue curve), but remains an equilibrium state with a tiny $\alpha = 0.005$. (b) Λ vs f for $\alpha = 0.005$ in region 1 (blue dots and the red line) and 2 (purple dots and the green line). Density plot of the Fourier transformation of $\varphi(x, t)$ in fk -plane shows spin waves spectrum in current-free (c) and current-flow (d) regions.

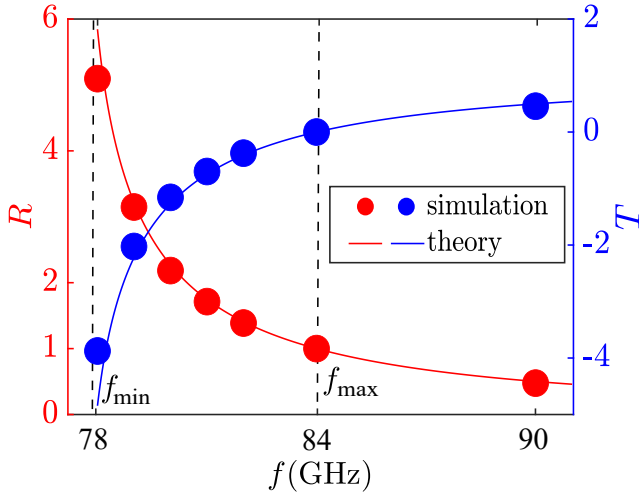


FIG. 3. Reflection and transmission coefficients as functions of f from simulations (red and blue dots) and theory (the red and blue line). Two dashed lines mark f_{\min} and f_{\max} , respectively.

easily be obtained,

$$R = \frac{|C|^2}{|B|^2} = \left(\frac{k_1 - k_2}{k_1 + k_2} \right)^2 \quad (6)$$

$$T = \frac{k_2 |D|^2}{k_1 |B|^2} = \frac{4k_1 k_2}{(k_1 + k_2)^2}.$$

If ω is in the inverted spectrum, $k_2 < 0$, $R > 1$ and negative $T < 0$ show the backward propagation. This super-reflection is confirmed from the micromagnetic simula-

tions as shown in Fig. 3 for $k_2 < 0$.

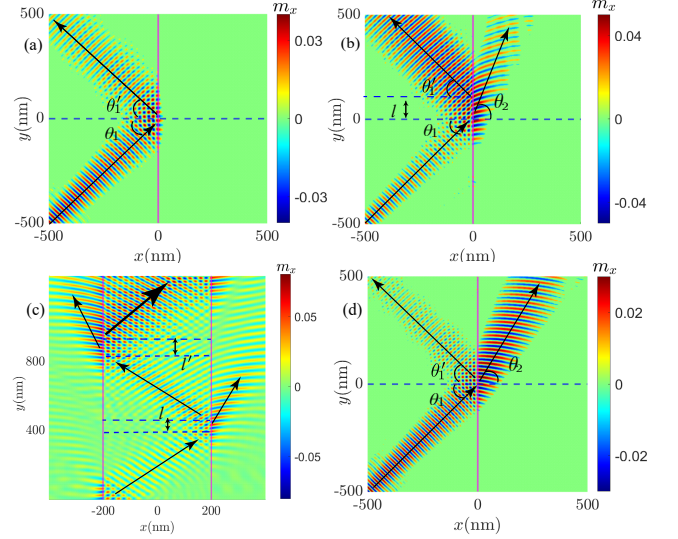


FIG. 4. Reflection and refraction of a spin wave of frequency $f = 100$ GHz and $\alpha = 0.001$ at the interface without (a) and with (b) a current density of $\vec{j} = 10^{13} \hat{x} \text{ A m}^{-2}$ in $x > 0$. The black arrowed lines mark the propagation directions of incident, reflective and refractive waves. $\theta_1 = \theta'_1 = 45^\circ$, $\theta_2 = 71^\circ$. (c) Spin wave intensity between two super-mirrors (purple lines). Along the reflection path (the red arrowed lines) the intensity of reflected wave increases. The current density on the left (right) region is $j = -10^{13} \hat{x} \text{ A m}^{-2}$ ($j = 10^{13} \hat{x} \text{ A m}^{-2}$). Wave frequency is $f = 105$ GHz and $\alpha = 0.001$. (d) Reflection and refraction of a spin wave of frequency $f = 120$ GHz and $\alpha = 0.001$. $\theta_1 = \theta'_1 = 45^\circ$, $\theta_2 = 61^\circ$.

Continuity conditions require incident, reflective, and refractive wave vectors $\vec{k}_1, \vec{k}'_1, \vec{k}_2$ in general case satisfy $k_{1y} = k'_{1y} = k_{2y}$. Denote θ_1, θ'_1 , and θ_2 incident, reflective, and refractive angles, respectively, they follow $\theta'_1 = \theta_1$ and the Snell's law [34], $v_1 \sin \theta_1 = v_2 \sin \theta_2$, where 1 and 2 stand for normal and pumped regions. v_1 and v_2 are the group velocities [35]. Figure 4(a) and (b) show the simulation results for a wave of $\theta_1 = 45^\circ$ and frequency $f = 100$ GHz, which is in the frequency gap of the right region ($x > 0$) for $\vec{j} = 0$ and is allowed with $\vec{j} = 10^{13} \hat{x} \text{ A m}^{-2}$. Because of the gap, there is no refractive wave when $\vec{j} = 0$ as shown in Fig. 4(a). The results also show $\theta'_1 = \theta_1$ and no amplification of the reflected wave since the region is normal for $\vec{j} = 0$. In the presence of $\vec{j} \neq 0$ when the wave spectrum is inverted in the right region, Fig. 4(b) shows clearly the amplification of the reflective wave, the presences of both reflective and refractive waves with $\theta'_1 = \theta_1$ and $v_1 \sin \theta_1 = v_2 \sin \theta_2$ (see Supplemental Material for details).

We further consider a spin wave of $\theta_1 = 45^\circ$ and $f = 105$ GHz propagating in a normal region of width 200 nm sandwiched between two pumped media with $\vec{j} = -10^{13} \hat{x} \text{ A m}^{-2}$ ($\vec{j} = 10^{13} \hat{x} \text{ A m}^{-2}$) on the left (right) side, corresponding to spin wave reflection by two super-

mirrors. Figure 4(c) shows clearly that spin waves are amplified each times when it is reflected in this flat cavity. In contrast to usual laser cavity where waves gain in a medium and lose at cavity mirror [36], spin waves gain at super-mirrors and lose in the medium. Thus, the new amplification principle is fundamentally different from existing approaches and is an ideal concept for microscopic wave amplifiers/lasers.

Reflected waves have lateral shifts of l as shown in Figs. 4(b) and 4(c) when f ($= 100, 105$ GHz) are in the inverted region of the pumped medium. Interestingly, such a shift is absent when f is in normal region $[\notin (f_{min}, f_{max})]$ as shown in Fig. 4(d) for $f = 120$ GHz $> f_{max}$. This shift is the Goos-Hänchen effect or Imbert-Fedorov effect [37]. In contrast to the shift that normally appears in the total reflection in optics for linearly and circularly polarized light, we observed here the shift in super-reflection.

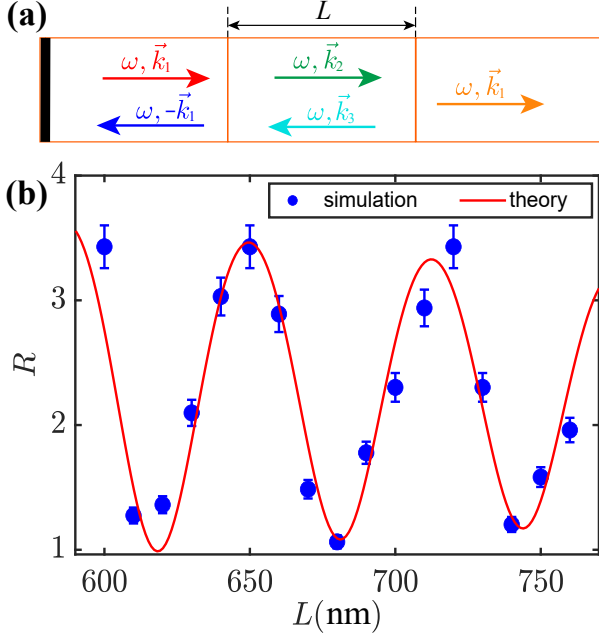


FIG. 5. (a) A sketch of wave propagation in a sandwiched structure with three regions. Current density of $\vec{j} = 10^{13} \hat{x} \text{ A m}^{-2}$ only flows in the middle region. (b) Reflection coefficient as a function of width L of the middle region. The wave frequency is $f = 80$ GHz, wave numbers are $k_1 = 0.16$ rad/nm, $k_2 = -0.03$ rad/nm, $k_3 = -0.13$ rad/nm, the damping coefficient $\alpha = 0.001$, decay constant $\Lambda_2 = 0.0008 \text{ nm}^{-1}$.

To gain further insight, we analyse a normally incident wave of ω and $\vec{k}_1 = (k_1, 0)$ from left to the right through a pumped region of width L sandwiched between two semi-infinite large normal regions. We assume that ω in the inverted spectrum region with corresponding two allowed wave vectors $\vec{k}_2 = (k_2 < 0, 0)$ and $\vec{k}_3 = (k_3 < 0, 0)$. In another work, incoming wave can activate two backward propagating waves in the pumped region. One of them (say k_2) has a positive group velocity (negative

phase velocity because of $k_2 < 0$), and the other (k_3) has both negative group and phase velocities. The spin wave function in the current case has the form,

$$\varphi = \begin{cases} B e^{-\Lambda_1 x} e^{i(\omega t - k_1 x)} + C e^{\Lambda_1 x} e^{i(\omega t + k_1 x)}, & x < 0 \\ D e^{-\Lambda_2 x} e^{i(\omega t - k_2 x)} + E e^{\Lambda_2 x} e^{i(\omega t - k_3 x)}, & 0 \leq x \leq L \\ F e^{-\Lambda_1 x} e^{i(\omega t - k_1 x)}. & x > L \end{cases} \quad (7)$$

The wave function should satisfy continuity conditions at both $x = 0$ and $x = L$. The four conditions determine uniquely reflection and transition coefficients,

$$R = \frac{|C|^2}{|B|^2} = \left| \frac{(k_1 - k_2)D + (k_1 - k_3)E}{(k_1 + k_2)D + (k_1 + k_3)E} \right|^2 \quad (8)$$

$$\frac{D}{E} = \frac{k_1 - k_3}{k_1 - k_2} e^{2\Lambda_2 L} e^{i[(k_3 - k_2)L + \pi]}$$

Eq. 6, $R = \left(\frac{k_1 - k_2}{k_1 + k_2}\right)^2$, is recovered by assuming $E = 0$. Eq. 8 shows that k_2 and k_3 can interfere with each other in the pumped region. The interference is constructive when $(k_2 - k_3)L = (2n + 1)\pi$ and destructive when $(k_2 - k_3)L = 2n\pi$, $n = \text{integer}$. Then the combined backward propagating modes interfere with the reflected wave, resulting in a super-reflection $R > 1$. Figure 5 shows how R oscillates with L with a period of $2\pi/|k_2 - k_3|$ for parameters defined above and $\alpha = 0.001$.

The amplification principle presented here is applicable to other waves such as electromagnetic and acoustic waves if similar conditions, such as inverted spectrum, an energy source, and proper boundary conditions, are satisfied. For spin waves, electric current can be the energy source, and it is well-established that current-induced STT can invert a spin wave spectrum.

Compare our spin wave amplification with other existing proposal, our proposal is not only universal, but also very easy to implement. Considering the typical spin wave devices are very small, super-mirror can be tens nano-meter in size. It may also be possible to use several super-mirrors to construct a spin wave cavity to make spin-wave “lasers”. Similar spin wave amplification by the interface of two coupled magnets has also been predicted recently [27]. However, the physics in Reference [27] is different from that presented here. Instead of physics of constructive interference of the reflective wave with incident refractive wave discussed here, Reference [27] associates the spin wave amplification from the Bosonic Klein paradox that involves the antimagnon, carrying opposite spin and energy. The spin-orbit torques was used to dynamically stabilize both magnons and antimagnons. In contrast, our theory is based on classical spin wave equations. The success of our proposal does not require any quantum effects such as quantum tunneling or particle-antiparticle concept and the Klein paradox. The spin transfer torques are used to invert spin wave spectrum. We would also like to point out that spin wave spectrum could also be

inverted with Dzyaloshinskii-Moriya interaction (DMI) [38, 39]. However, the boundary condition of DMI system requires discontinuity in the first derivative of spin wave at the boundary [40]. This discontinuity denied the spin wave amplification discussed here, in agreement with the physics principle that spin wave amplification require energy source.

In summary, we demonstrate that an interface between a current-free region and a current-flow region can be a super-mirror such that reflection coefficient can be larger than 1. The physics is the refractive wave in a pumped medium is a backward propagating wave that can constructively interfere with the reflected wave. The effective role of the pumped medium is to coherently emit energy to the reflected wave, leading to the superradiance of a super-mirror. The proposed physics and picture are verified by the micromagnetic simulations.

This work is supported by the National Key Research and Development Program of China Grant No. 2020YFA0309600, the National Natural Science Foundation of China (Grant No. 11974296) and Hong Kong RGC Grants (No. 16301518, No. 16301619, No. 16302321, and No. 16300522).

* Corresponding author: phxwan@ust.hk

- [1] H. Y. Yuan, Y. S. Cao, A. Kamra, R. A. Duine and P. Yan, Quantum magnonics: When magnon spintronics meets quantum information science, *Physics Reports*, **965**: 1-74 (2022).
- [2] X. S. Wang, P. Yan, Y. H. Shen, G. E. W. Bauer, and X. R. Wang, structure Wall Propagation through Spin Wave Emission, *Phys. Rev. Lett.* **109**, 167209 (2012).
- [3] P. Yan, X. S. Wang, and X. R. Wang, All-Magnonic Spin-Transfer Torque and structure Wall Propagation, *Phys. Rev. Lett.* **107**, 177207 (2011).
- [4] X. S. Wang, H. W. Zhang, and X. R. Wang, Topological Magnonics: A Paradigm for Spin-Wave Manipulation and Device Design, *Phys. Rev. Applied* **9**, 024029 (2018).
- [5] A. V. Chumak, A. A. Serga, and B. Hillebrands, Magnon transistor for all-magnon data processing. *Nat. Commun.* **5**, 4700 (2014).
- [6] G. Csaba, A. Papp, and W. Porod, Perspectives of using spin waves for computing and signal processing, *Phys. Lett. A*, **381**, 1471 (2017).
- [7] A. Barman, G. Gubbiotti, S. Ladak, et al, The 2021 magnonics roadmap, *J. Phys.: Condens. Matter*, **33** 413001 (2021).
- [8] I. Bertelli, J. J. Carmiggelt, T. Yu, et al. Magnetic resonance imaging of spin-wave transport and interference in a magnetic insulator, *Sci. Adv.* **6**, 46 (2020).
- [9] C. Liu, J. Chen, T. Liu, F. Heimbach, H. Yu, Y. Xiao, J. Hu, M. Liu, H. Chang, T. Stueckler, S. Tu, Y. Zhang, Y. Zhang, P. Gao, Z. Liao, D. Yu, K. Xia, N. Lei, W. Zhao, and M. Wu, Long-distance propagation of short-wavelength spin waves, *Nat. Commun.* **9**, 738 (2018).
- [10] E. Padrón-Hernández, A. Azevedo, and S. M. Rezende, Amplification of Spin Waves by Thermal Spin-Transfer Torque, *Phys. Rev. Lett.* **107**, 197203 (2011).
- [11] S. M. Seo, K. J. Lee, H. Yang, and T. Ono, Current-Induced Control of Spin-Wave Attenuation, *Phys. Rev. Lett.* **102**, 147202 (2009).
- [12] K. An, D. R. Birt, C. F. Pai, K. Olsson, D. C. Ralph, R. A. Buhrman, and X. Q. Li, Control of propagating spin waves via spin transfer torque in a metallic bilayer waveguide, *Phys. Rev. B*, **89**, 140405 (2014).
- [13] S. Woo and G. S. D. Beach, Control of propagating spin-wave attenuation by the spin-Hall effect. *J. Appl. Phys.* **122**, 093901 (2017).
- [14] B. Divinskiy, V. E. Demidov, S. Urazhdin, R. Freeman, A. B. Rinkevich, and S. O. Demokritov, Excitation and amplification of spin waves by spin-orbit torque, *Adv. Mater.* **30**, 1802837 (2018).
- [15] V. E. Demidov, S. Urazhdin, A. Anane, V. Cros, and S. O. Demokritov, Spin-orbit-torque magnonics, *J. Appl. Phys.* **127**, 170901 (2020).
- [16] A. I. Nikitchenko and N. A. Pertsev, Spin-orbit torque control of spin waves in a FM waveguide, *Phys. Rev. B* **104**, 134422 (2021).
- [17] H. Merbouche, B. Divinskiy, D. Gouéré, R. Lebrun, A. El-Kanj, V. Cros, P. Bortolotti, A. Anane, S. O. Demokritov, and V. E. Demidov, True amplification of spin waves in magnonic nano-waveguides, [arXiv:2303.04695](https://arxiv.org/abs/2303.04695) (2023).
- [18] P. A. Kolodin, P. Kabos, C. E. Patton, B. A. Kalinikos, N. G. Kovshikov, and M. P. Kostylev, Amplification of microwave magnetic envelope solitons in thin yttrium iron garnet films by parallel pumping, *Phys. Rev. Lett.* **80**, 1976 (1998).
- [19] T. Brächer, P. Pirro, and B. Hillebrands, Parallel pumping for magnon spintronics: Amplification and manipulation of magnon spin currents on the micron-scale, *Phys. Rep.* **699**, 1 (2017).
- [20] B. Heinz, M. Mohseni, A. Lentfert, R. Verba, M. Schneider, B. Lägél, K. Levchenko, T. Brächer, C. Dubs, A. V. Chumak, and P. Pirro, Parametric generation of spin waves in nanoscaled magnonic conduits, *Phys. Rev. B* **105**, 144424 (2022).
- [21] P. Chowdhury, P. Dhagat, and A. Jander, Parametric amplification of spin waves using acoustic waves, *IEEE Trans. Magnet.* **51**, 1300904 (2015).
- [22] P. Graczyk, M. Krawczyk, Coupled mode theory for the acoustic wave and spin wave interaction in the magnonic crystals: Propagating magnetoelastic waves, *Phys. Rev. B* **96**, 024407 (2017).
- [23] R. Verba, V. Tiberkevich, I. Krivorotov, and A. Slavin, Parametric Excitation of Spin Waves by Voltage-Controlled Magnetic Anisotropy, *Phys. Rev. Appl.* **1**, 044006 (2014).
- [24] O. Klein, Die Reflexion von Elektronen an einem Potentialsprung nach der relativistischen Dynamik von Dirac, *Zeitschrift für Physik* **53**, 157 (1929).
- [25] R. Brito, V. Cardoso, P. Pani, Superradiance, *Lect. Notes Phys.* **906**, 1-237 (2015).
- [26] R. J. Doornenbal, A. Roldán-Molina, A. S. Nunez, and R. A. Duine, Spin-wave amplification and lasing driven by inhomogeneous spin-transfer torques, *Phys. Rev. Lett.* **122**, 037203(2019).
- [27] J. S. Harms, H. Y. Yuan, and R. A. Duine, Enhanced magnon spin current using the bosonic Klein paradox, *Phys. Rev. Applied* **18**, 064026 (2022)
- [28] Z. Y. Wang, H. Y. Yuan, Y. S. Cao, and P. Yan, Twisted

- Magnon Frequency Comb and Penrose Superradiance, *Phys. Rev. Lett.* **129**, 107203 (2022).
- [29] X. C. Hu, H. T. Wu, X. R. Wang, A theory of skyrmion crystal formation, *Nanoscale*, **14**, 7516 (2022).
- [30] Excitation of a magnetic multilayer by an electric current M. Tsoi, A. G. M. Jansen, J. Bass, W.-C. Chiang, M. Seck, V. Tsoi, and P. Wyder, *Phys. Rev. Lett.* **80**, 4281 (1998)
- [31] Y. Ji, C. L. Chien, and M. D. Stiles, Current-induced spin-wave excitations in a single ferromagnetic layer, *Phys. Rev. Lett.* **90**, 106601 (2003)
- [32] A. Vansteenkiste, J. Leliaert, M. Dvornik, M. Helsen, F. G. Sanchez, and B. V. Waeyenberge, The design and verification of MuMax3, *AIP Advances* **4**, 107133 (2014).
- [33] X. R. Wang, P. Yan, J. Lu, and C. He, Magnetic field driven domain-wall propagation in magnetic nanowires, *Ann. Phys. (NY)* **8**, 324, 1815 (2009).
- [34] J. Mulkers, B. Van Waeyenberge, and M. V. Milošević, Tunable Snell's law for spin waves in heterochiral magnetic films, *Phys. Rev. B* **97**, 104422 (2018).
- [35] In simulations, incoming wave packets around frequency ω and wave vector $\vec{k}_1 = (k_{1x}, k_{1y})$ at the incident angle θ_1 is reflected and refracted at the interface. The reflected wave packet of frequency ω and wave vector $\vec{k}'_1 = (-k_{1x}, k_{1y})$ travel along its group velocity at the reflective angle $\theta'_1 = \theta_1$ while the refracted wave packet of frequency ω and wave vector $\vec{k}_2 = (k_{2x}, k_{2y})$ travel along its group velocity at refractive angle θ_2 . In contrast to the Snell law in optics where the phase velocities are involved, the Snell law for spin wave packets refraction is determined by their group velocities because of their nonlinear wave spectrum.
- [36] G. Kim, S. H. Song, J. W. Yoon, Inverse-cavity structure for low-threshold miniature lasers, *Sci. Rep.*, **12**, 11333 (2022).
- [37] X. Yin, Goos-Hänchen shift surface plasmon resonance sensor, *Appl. Phys. Lett.* **89**, 261108 (2006).
- [38] R. L. Melcher, Linear contribution to spatial dispersion in the spin-wave spectrum of ferromagnets *Phys. Rev. Lett.* **30**, 125 (1973).
- [39] J.-H. Moon, S.-M. Seo, K.-J. Lee, K.-W. Kim, J. Ryu, H.-W. Lee, R. D. McMichael, and M. D. Stiles, Spin-wave propagation in the presence of interfacial Dzyaloshinskii-Moriya interaction, *Phys. Rev. B* **88**, 184404 (2013).
- [40] S. Rohart and A. Thiaville, Skyrmion confinement in ultrathin film nanostructures in the presence of Dzyaloshinskii-Moriya interaction, *Phys. Rev. B* **88**, 184422 (2013).

Supplemental materials for: Spin wave amplification through superradiance

X. R. Wang,^{1,2,3,*} X. Gong,¹ and K. Y. Jing¹

¹Physics Department, The Hong Kong University of Science and Technology, Clear Water Bay, Kowloon, Hong Kong

²HKUST Shenzhen Research Institute, Shenzhen 518057, China

³William Mong Institute of Nano Science and Technology,

The Hong Kong University of Science and Technology, Clear Water Bay, Kowloon, Hong Kong, China

The supplemental materials include 1) Derivation of spin wave continuity condition at interface 2) Derivation of reflection coefficient of 1D super-mirror and cavity between two super-mirrors, 3) Derivation of the Snell's law and its numerical verification, 4) Numerical determinations of spin wave spectrum, reflection and transmission coefficients. 5) The effect of nonadiabatic STT. 6) An additional micromagnetic simulation of wave amplification in doped permalloy.

1. Derivation of spin wave continuity condition at interface

$\varphi \equiv m_x + im_y$ must be continue at interface because m_x, m_y are continuous, or $\varphi(x = 0^-) = \varphi(x = 0^+)$. Otherwise, the governing spin-wave dynamical equation (4) in the main text will contain high order divergent terms. To obtain the boundary condition for the derivatives of φ , we integrate Eq. (4) over a volume near the boundary of current-free and current-flow regions. For the simplicity, we use 1D as an example. The integral along x -direction is

$$\int_{-\varepsilon}^{\varepsilon} -i \frac{\partial \varphi}{\partial t} dx = \frac{1 + i\alpha}{1 + \alpha^2} \int_{-\varepsilon}^{\varepsilon} (-A' \nabla^2 + K' + i\vec{u} \cdot \nabla) \varphi dx. \quad (1.1)$$

As $\varepsilon \rightarrow 0$, the term on left-hand side

$$\lim_{\varepsilon \rightarrow 0} \int_{-\varepsilon}^{\varepsilon} \frac{\partial \varphi}{\partial t} dx = 0, \quad (1.2)$$

the first and second term on right-hand side

$$\lim_{\varepsilon \rightarrow 0} \int_{-\varepsilon}^{\varepsilon} A' \nabla^2 \varphi dx = \lim_{\varepsilon \rightarrow 0} A' \left. \frac{\partial \varphi}{\partial x} \right|_{-\varepsilon}^{\varepsilon} = A' \left[\frac{\partial \varphi}{\partial x}(x = 0^+) - \frac{\partial \varphi}{\partial x}(x = 0^-) \right], \quad (1.3)$$

$$\lim_{\varepsilon \rightarrow 0} \int_{-\varepsilon}^{\varepsilon} K' \varphi dx = \lim_{\varepsilon \rightarrow 0} \left(K'(x < 0) \int_{-\varepsilon}^0 \varphi dx + K'(x \geq 0) \int_0^{\varepsilon} \varphi dx \right) = 0, \quad (1.4)$$

Integrating the third term on right-hand side by parts gives

$$\lim_{\varepsilon \rightarrow 0} \int_{-\varepsilon}^{\varepsilon} (\vec{u} \cdot \nabla) \varphi dx = \lim_{\varepsilon \rightarrow 0} u \varphi \Big|_{-\varepsilon}^{\varepsilon} - \lim_{\varepsilon \rightarrow 0} \int_{-\varepsilon}^{\varepsilon} \varphi \nabla \cdot \vec{u} dx. \quad (1.5)$$

Since $\vec{u} = 0(x < 0)$, $\vec{u} = u\hat{x}(x \geq 0)$, $\frac{\partial \vec{u}}{\partial x} = u\delta(x)\hat{x}$,

$$\lim_{\varepsilon \rightarrow 0} u \varphi \Big|_{-\varepsilon}^{\varepsilon} = \lim_{\varepsilon \rightarrow 0} u(\varepsilon)\varphi(\varepsilon) - u(-\varepsilon)\varphi(-\varepsilon) = \lim_{\varepsilon \rightarrow 0} u(\varepsilon)\varphi(\varepsilon) - 0 = u\varphi(x = 0), \quad (1.6)$$

and

$$\lim_{\varepsilon \rightarrow 0} \int_{-\varepsilon}^{\varepsilon} \varphi \nabla \cdot \vec{u} dx = \lim_{\varepsilon \rightarrow 0} \int_{-\varepsilon}^{\varepsilon} \varphi u \delta(x) dx = u\varphi(x = 0). \quad (1.7)$$

There is another way to see $\nabla \varphi(0^-) = \nabla \varphi(0^+)$ directly from Eq. (4). Since all terms, except possibly the first term on the right hand side, in the equation are finite (the last term on the right hand side can at most be a step function), the tiny integrals around boundary must be order of infinitesimal volume. To the zero order in the small volume, the integral is $A[\nabla \varphi(0^+) - \nabla \varphi(0^-)] = 0$, which is the claimed boundary condition.

* Corresponding author: phxwan@ust.hk

2. Derivation of reflection coefficient of 1D super-mirror and cavity between two super-mirrors

For a wave propagating from the left to the right along the x -direction in one dimensional space with an interface at $x = 0$ which separates two homogeneous media with different material parameters, the wave function of frequency ω is, due to the reflection and refraction,

$$\varphi = \begin{cases} B e^{-\Lambda_1 x} e^{i(\omega t - k_1 x)} + C e^{\Lambda_1 x} e^{i(\omega t + k_1 x)}, & x < 0 \\ D e^{-\Lambda_2 x} e^{i(\omega t - k_2 x)}, & x \geq 0. \end{cases} \quad (2.1)$$

k_1 and $-k_1$ are two corresponding wave vectors of ω in medium 1 on the left, corresponding to the forward and backward propagating waves. k_2 is one of two wave vectors of ω in medium 2 on the right side of the interface whose group velocity is toward the right. Λ_i^{-1} ($i = 1, 2$) is the decay length in medium i . φ satisfies the continuity conditions at the interface ($x = 0$), $\varphi(x = 0^-) = \varphi(x = 0^+)$ and $\nabla\varphi(x = 0^-) = \nabla\varphi(x = 0^+)$. Thus,

$$\begin{aligned} B + C &= D, \\ (-ik_1 - \Lambda_1)B + (ik_1 + \Lambda_1)C &= (-ik_2 - \Lambda_2)D. \end{aligned} \quad (2.2)$$

$\frac{C}{B} = \frac{(k_1 - i\Lambda_1) - (k_2 - i\Lambda_2)}{(k_1 - i\Lambda_1) + (k_2 - i\Lambda_2)}$, $\frac{D}{B} = \frac{2(k_1 - i\Lambda_1)}{(k_1 - i\Lambda_1) + (k_2 - i\Lambda_2)}$. When the decay lengths are much larger than the wavelength, the reflection and transmission coefficients are

$$\begin{aligned} R &= \frac{|C|^2}{|B|^2} = \left(\frac{k_1 - k_2}{k_1 + k_2} \right)^2 \\ T &= \frac{k_2 |D|^2}{k_1 |B|^2} = \frac{4k_1 k_2}{(k_1 + k_2)^2}. \end{aligned} \quad (2.3)$$

In the case of a wave propagating from the left to the right through two super-mirrors at $x = 0$ and $x = L$, respectively, which consists of a pumped medium in the middle ($0 \leq x \leq L$) and two identical normal media on the two sides, φ is,

$$\varphi = \begin{cases} B e^{-\Lambda_1 x} e^{i(\omega t - k_1 x)} + C e^{\Lambda_1 x} e^{i(\omega t + k_1 x)}, & x < 0 \\ D e^{-\Lambda_2 x} e^{i(\omega t - k_2 x)} + E e^{\Lambda_2 x} e^{i(\omega t - k_3 x)}, & 0 \leq x \leq L \\ F e^{-\Lambda_1 x} e^{i(\omega t - k_1 x)}, & x > L \end{cases} \quad (2.4)$$

where k_2 and k_3 are assumed to be two negative wave vectors in the pumped media. The spectrum has a positive group velocity at k_2 and a negative group velocity at k_3 . The boundary conditions yield

$$\begin{aligned} B + C &= D + E \\ (k_1 - i\Lambda_1)B - (k_1 - i\Lambda_1)C &= (k_2 - i\Lambda_2)D + (k_3 + i\Lambda_2)E \\ D e^{-\Lambda_2 L} e^{-ik_2 L} + E e^{\Lambda_2 L} e^{-ik_3 L} &= F e^{-\Lambda_1 L} e^{-ik_1 L} \\ (k_2 - i\Lambda_2)D e^{-\Lambda_2 L} e^{-ik_2 L} + (k_3 + i\Lambda_2)E e^{\Lambda_2 L} e^{-ik_3 L} &= (k_1 - i\Lambda_1)F e^{-\Lambda_1 L} e^{-ik_1 L}. \end{aligned} \quad (2.5)$$

In terms of $k_1, k_2, k_3 \gg \Lambda_1, \Lambda_2$, we have

$$\begin{aligned} R &= \frac{|C|^2}{|B|^2} = \left| \frac{(k_1 - k_2)D + (k_1 - k_3)E}{(k_1 + k_2)D + (k_1 + k_3)E} \right|^2 \\ \frac{D}{E} &= -\frac{k_1 - k_3}{k_1 - k_2} e^{2\Lambda_2 L} e^{i(k_3 - k_2)L}. \end{aligned} \quad (2.6)$$

3. Derivation of the Snell's law and its numerical verification

For a spin wave of frequency ω with incident angle θ_1 in a two-dimensional plane, the wave function is

$$\varphi = \begin{cases} B e^{-\Lambda_1 x} e^{i(\omega t - \vec{k}_1 \cdot \vec{r})} + C e^{\Lambda_1 x} e^{i(\omega t - \vec{k}_1' \cdot \vec{r})}, & x < 0 \\ D e^{-\Lambda_2 x} e^{i(\omega t - \vec{k}_2 \cdot \vec{r})}, & x \geq 0 \end{cases} \quad (3.1)$$

where $|\vec{k}_1| = |\vec{k}'_1|$ and $k_{1,x} = -k'_{1,x}$ for spectrum in current-free region. \vec{k}_2 is the wave vector of frequency ω whose group velocity is forward (positive). From the boundary conditions of $\varphi(x=0^-) = \varphi(x=0^+)$ and $\nabla\varphi(x=0^-) = \nabla\varphi(x=0^+)$, we have

$$\begin{aligned} Be^{-ik_{1,y}y} + Ce^{-ik'_{1,y}y} &= De^{-ik_{2,y}y} \\ \vec{k}_1 Be^{-ik_{1,y}y} + \vec{k}'_1 Ce^{-ik'_{1,y}y} &= \vec{k}_2 De^{-ik_{2,y}y}. \end{aligned} \quad (3.2)$$

Above equations are true for an arbitrary y only when $k_{1,y} = k'_{1,y} = k_{2,y}$. Here we are dealing with a wave packet centred around frequency ω which is emitted from a source located at the lower left corner of the sample as shown in Fig. 1 in the main text. The wave-packet propagates along group velocity of $\vec{v}_2 = 2A'\vec{k}_2 + \vec{u}$ in the pumped region while the incident and reflective waves propagate along $\vec{v}_1 = 2A'\vec{k}_1$ and $\vec{v}'_1 = 2A'\vec{k}'_1$, respectively. If θ_1 , θ'_1 , and θ_2 are defined as incident, reflective, and refractive angles (the angle between group velocity and \hat{x}), then we have $v_{1,y} = v'_{1,y} = v_{2,y}$, $\theta_1 = \theta'_1$, and

$$v_1 \sin \theta_1 = v_2 \sin \theta_2. \quad (3.3)$$

To verify the correctness of the Snell's law, we consider a film of $2000 \times 2000 \times 2\text{nm}^3$ centred at the origin of xy -plane. All model parameters are the same as those in the main text, and the left-half of the film is current-free while the right-half of the film has current flowing to the x -direction. We use MuMax3 to solve the LLG equation with an oscillating magnetic field of frequency ω applied on a strip of $100\text{nm} \times 4\text{nm}$ which is placed at the lower-left corner of the film at various inclined angles with respect to y -axis. In order to eliminate un-wanted spin wave reflection from the film boundary, the damping coefficient at the boundaries is assumed to be 0.5. The generated spin wave propagates toward the interface at an arbitrary incident angle θ_1 that is determined by the inclined angle of the strip. After the magnetization reaches its stable distribution, $\vec{m}(\vec{x}) \cos[\omega t - \phi(\vec{x})]$, we use those $|m_x(x, y)| > 0.2 \max(|m_x(x, y)|)$ or $|m_y(x, y)| > 0.2 \max(|m_y(x, y)|)$ to compute the incident, reflective and refractive spin wave beams. We then numerically search y 's such that $|\vec{m}(x, y)|$ is the local maxima for a given x . The beam directions are defined as the lines connecting all these local maximal field points. The incident, reflective and refractive angles can then easily be obtained from the beam directions. Wave vector $\vec{k} = (k_x, k_y)$ is obtained through the two-dimensional Fourier transformation $m_x(x, y) \rightarrow \tilde{m}_x(k_x, k_y)$ (the peak position of $|\tilde{m}_x(k_x, k_y)|^2$ is defined as k_x and k_y). The group velocity is then obtained from the formula $v = \sqrt{(2A'k_x)^2 + (2A'k_y)^2}$ (current-free region) or $\sqrt{(2A'k_x + u)^2 + (2A'k_y)^2}$ (current-flow region). The results are listed in Table. S1, which follows the Snell's law (Eq. 3.3).

TABLE S1. Incident angles θ_1 , refractive angles θ_2 , group velocities in medium 1 (v_1) and in medium 2 (v_2)

Frequency f (GHz)	Incident angle θ_1	Refractive angle θ_2	v_1 (m/s)	v_2 (m/s)	$v_1 \sin \theta_1$ (m/s)	$v_2 \sin \theta_2$ (m/s)
90	30°	57°	2239	1348	1120	1130
100	45°	71°	2544	1881	1799	1778
110	45°	65°	2821	2183	1995	1978
120	45°	61°	3072	2498	2172	2184

4. Numerical determinations of spin wave spectrum, reflection and transmission coefficients

Spin wave spectrum of a given system can be extracted from a thermally activated magnetization fluctuation around its equilibrium state from the Fourier transformation of the fluctuation as used in our previous studies [S1–S4]. We use a magnetic strip of $2000 \times 2 \times 2\text{nm}^3$ as an example to illustrate the procedures. The material parameters are the same as those given in the main text. At a finite temperature, magnetization can feel a thermal field of $\vec{h} = \vec{\eta} \sqrt{2\alpha k_B T / (M_s \mu_0 \gamma \Delta V \Delta t)}$, where ΔV , Δt , T and $\vec{\eta}$ are the cell volume, time step, temperature, and a random vector from a standard normal distribution, respectively [S5, S6]. MuMax3 is used to generate magnetization fluctuation around its thermal equilibrium state. Starting from an initial magnetization state of $\vec{m} = \hat{z}$, magnetization will soon (in nanoseconds) reaches its thermal equilibrium states. $m_x(x, t)$ and $m_y(x, t)$ are then recorded every 0.5ps for 1ns. This shall allow us to find spin wave spectrum for frequencies between $f = 1\text{GHz}$ to $f = 2\text{THz}$. From the Fourier transform $\tilde{\varphi}(k, f)$ of $\varphi(x, t) \equiv m_x(x, t) + im_y(x, t)$, the spectral intensity function is then the square of its magnitude, $|\tilde{\varphi}(k, f)|^2$. The spin wave spectrum can then easily be obtained from the density plot of $|\tilde{\varphi}(k, f)|^2$ as a color map in fk -plane, as shown in Fig. 2(c) and (d) in the main text.

To simulate reflection and refraction of a normally incident spin wave, an oscillating magnetic field $\mu_0 \vec{H} = 0.5 \sin(\omega t) \hat{x} \text{T}$ is applied in a $32 \times 4\text{nm}^2$ strip on the left boundary of the current-free region. The film size is $2000 \times 32 \times 2\text{nm}^3$. We choose f in the range of [78, 90] GHz, which covers both the frequency gap and inverted frequency in the pumped region. When the system reaches a dynamic equilibrium, spin wave $\varphi(x, t) = \frac{1}{10} \sum_y m_x(x, y, t) + im_y(x, y, t)$ is then obtained. Then we use the Prony method

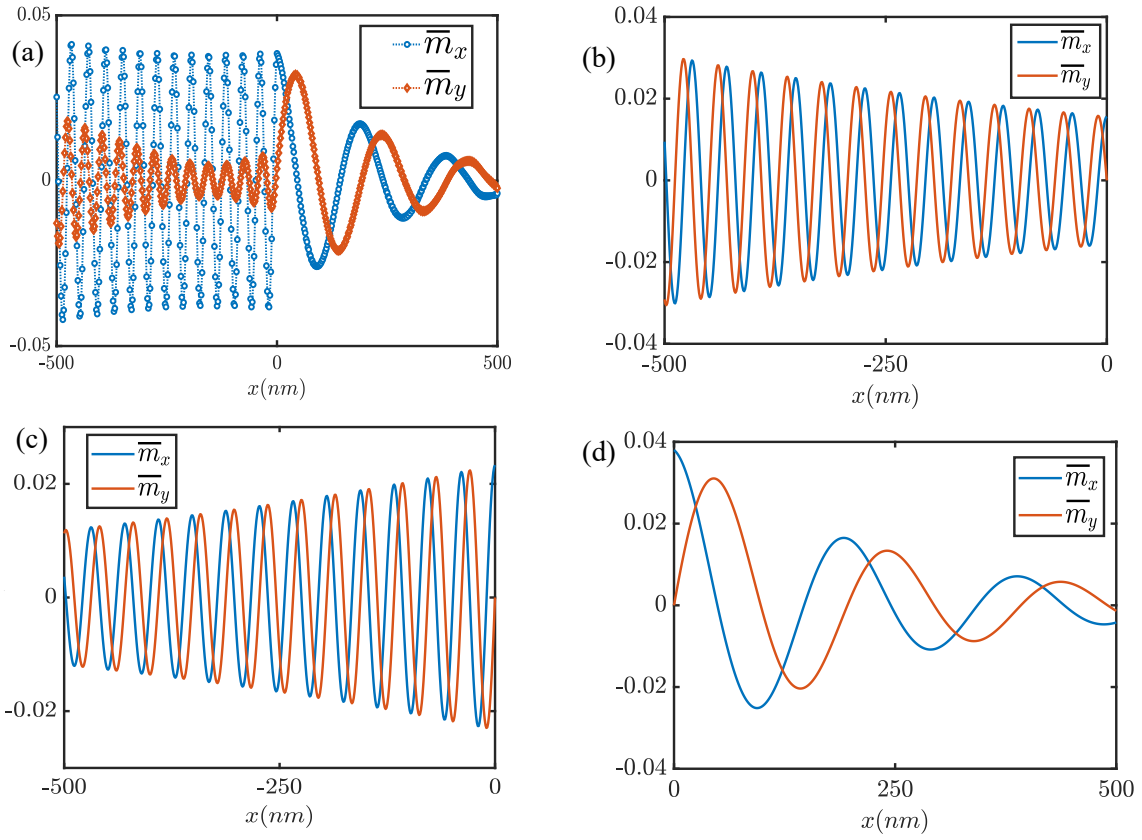


FIG. S1. (a) A snap-shot of spin wave of $\bar{m}_x \equiv \frac{1}{16} \sum_y m_x(x, y)$ and $\bar{m}_y \equiv \frac{1}{16} \sum_y m_y(x, y)$ at $t = 2\text{ns}$. $f = 80\text{GHz}$ is used. The interface between the current-free region (left) and current-flow region (right) is at $x = 0$. (b) The incident wave. (c) The reflective wave. (d) The refractive wave.

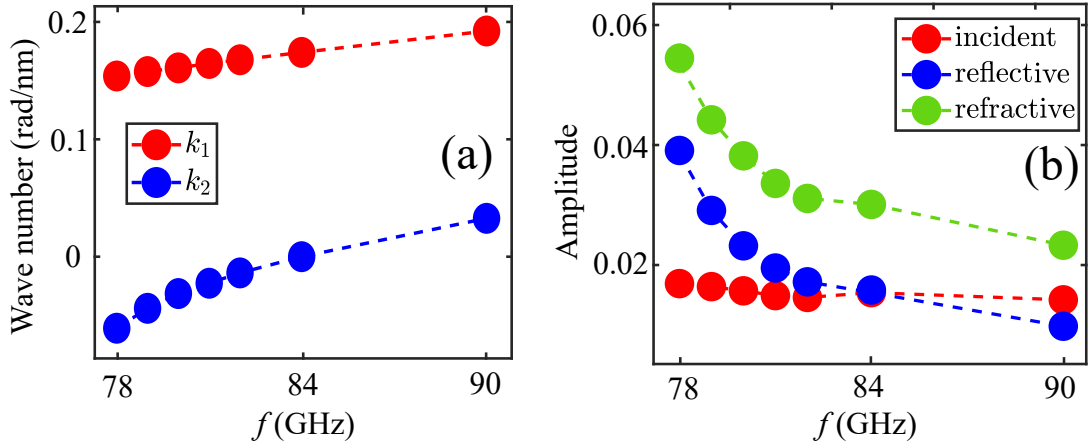


FIG. S2. (a) Wave numbers k_1 (red dots) and k_2 (blue dots) dependence on frequency obtained from simulations. (b) Amplitudes of the incident wave (red dots), reflective wave (blue dots), and refractive wave (green dots) for spin wave with different frequencies.

[S7] (fitting the data by wave function Eq. 2.1) to separate the incident, reflective and refractive waves. The results are shown in Fig. S1. The Prony method allows us to extract $|B|$, $|C|$, $|D|$, k_1 , k_2 , Λ_1^{-1} , and Λ_2^{-1} which are plotted in Fig. S2. The reflection and transmission coefficients defined as $R = |C|^2/|B|^2$ and $T = k_2|D|^2/(k_1|B|^2)$ are given in Fig. 3 in the main text.

5. The effect of non-adiabatic STT

In this section, we add a non-adiabatic STT, $\beta\vec{m} \times (\vec{u} \cdot \nabla)\vec{m}$, to the LLG equation, and investigate how it affects the spin wave amplification. The dynamic equation of m_x and m_y in current-flow region becomes

$$\begin{pmatrix} \partial_t + \vec{u} \cdot \nabla & -A'\nabla^2 + K' + \alpha\partial_t + \beta\vec{u} \cdot \nabla \\ A'\nabla^2 - K' - \alpha\partial_t - \beta\vec{u} \cdot \nabla & \partial_t + \vec{u} \cdot \nabla \end{pmatrix} \begin{pmatrix} m_x \\ m_y \end{pmatrix} = 0. \quad (5.1)$$

Then the dispersion relation is

$$\omega - i\alpha\omega = A'|\vec{k} - i\vec{\Lambda}|^2 + \vec{u} \cdot (\vec{k} - i\vec{\Lambda}) + K' - i\beta\vec{u} \cdot (\vec{k} - i\vec{\Lambda}). \quad (5.2)$$

Taking one-dimensional case as an example, the equation becomes

$$A' \left(k + \frac{u}{2A'} \right)^2 = \omega - K' + \frac{u^2}{4A'} + A'\Lambda^2 + \beta u\Lambda, \quad (5.3a)$$

$$(2A'k + u)\Lambda = \alpha\omega - \beta uk. \quad (5.3b)$$

For a given ω , the corresponding wave number of refractive wave takes the solution

$$\begin{aligned} k_2 - i\Lambda_2 &= \frac{-(u - i\beta u) + \sqrt{(u - i\beta u)^2 + 4A'(\omega - i\alpha\omega - K'_2)}}{2A'} \\ &= \frac{-(u - i\beta u) + \sqrt{u^2 - \beta^2 u^2 + 4A'(\omega - K'_2) - i(2\beta u^2 + 4A'\alpha\omega)}}{2A'} \\ &= \frac{u}{2A'} \left[-1 + i\beta + \sqrt{1 - \beta^2 + 4A'(\omega - K'_2)/u^2 - i(2\beta + 4A'\alpha\omega/u^2)} \right]. \end{aligned} \quad (5.4)$$

Define $a = 1 - \beta^2 + 4A'(\omega - K'_2)/u^2$, $b = 2\beta + 4A'\alpha\omega/u^2$. In most realistic cases [S8–S14], $\alpha, \beta \ll 1$, $b/a \ll 1$, then we can expand the square root term to the second order of b/a :

$$\sqrt{1 - \beta^2 + 4A'(\omega - K'_2)/u^2 - i(2\beta + 4A'\alpha\omega/u^2)} = \sqrt{a - bi} \approx \sqrt{a} \left(1 - \frac{bi}{2a} + \frac{b^2}{8a^2} \right). \quad (5.5)$$

Thus,

$$\Lambda_2 = \frac{u}{2A'} \left(-\beta + \sqrt{a} \frac{b}{2a} \right) = \frac{u}{2A'} \left[\frac{2A'\alpha\omega}{u^2 \sqrt{a}} + \beta \left(\frac{1}{\sqrt{a}} - 1 \right) \right]. \quad (5.6)$$

Under the condition of superradiance, $k_2 < 0$, $\omega < K'_2$, $a < 1$, the term proportional to β in the square bracket is positive, indicating an increase of decay constant Λ_2 from non-adiabatic STT. Further, the increase of Λ_2 leads to a subsequent rise in $A'\Lambda_2^2 + \beta u\Lambda_2$, resulting in an increase of k_2 (less negative), as seen from Eq. 5.3(a). For the wave number,

$$k_2 = \frac{u}{2A'} \left(-1 + \sqrt{a} + \sqrt{a} \frac{b^2}{8a^2} \right). \quad (5.7)$$

Using relations

$$\left(\sqrt{a} + \sqrt{a} \frac{b^2}{8a^2} \right)^2 > a + \frac{b^2}{4a}, \quad (5.8)$$

and

$$\frac{b^2}{4a} = \frac{(2\beta + 4A'\alpha\omega/u^2)^2/4}{1 - \beta^2 + 4A'(\omega - K'_2)/u^2} > \frac{\beta^2}{1 - \beta^2 + 4A'(\omega - K'_2)/u^2}, \quad (5.9)$$

one has

$$\left(\sqrt{a} + \sqrt{a} \frac{b^2}{8a^2} \right)^2 > 1 - \beta^2 + 4A'(\omega - K'_2)/u^2 + \frac{\beta^2}{1 - \beta^2 + 4A'(\omega - K'_2)/u^2} = 1 + 4A'(\omega - K'_2)/u^2 + \beta^2 \left(\frac{1}{a} - 1 \right) > 1 + 4A'(\omega - K'_2)/u^2, \quad (5.10)$$

and

$$-1 + \sqrt{a} + \sqrt{a} \frac{b^2}{8a^2} > -1 + \sqrt{1 + 4A'(\omega - K_2')/u^2}. \quad (5.11)$$

Thus,

$$k_2 > \frac{u}{2A'} \left[-1 + \sqrt{1 + 4A'(\omega - K_2')/u^2} \right], \quad (5.12)$$

value of k_2 in the presence of β is larger (less negative) than that in the absence of β . We can conclude that the presence of the non-adiabatic STT leads to an increase of wave number.

Since Λ_2 is not negligible, the exact reflection coefficient should be

$$R = \left| \frac{k_1 - k_2 + i\Lambda_2}{k_1 + k_2 - i\Lambda_2} \right|^2 = \frac{(k_1 - k_2)^2 + \Lambda_2^2}{(k_1 + k_2)^2 + \Lambda_2^2}. \quad (5.13)$$

When $k_1 > 0$, $k_2 < 0$, the increasing of Λ_2 and k_2 will lead to the reduction of R .

These analysis (solid lines in Fig. S3) are verified by micromagnetic simulations (dots in Fig. S3). From Fig. S3 (a,b), we can see that for a given frequency, the Λ_2 and k_2 increase with increasing β , and reflection coefficient decreases with the increase of β , in agreement with our theoretical analysis not only qualitatively, but also quantitatively. The range of β is taken as $[0, 40\alpha]$, as in most common materials [S8–S14]. For extremely large β above this range, dynamical instabilities may occur.

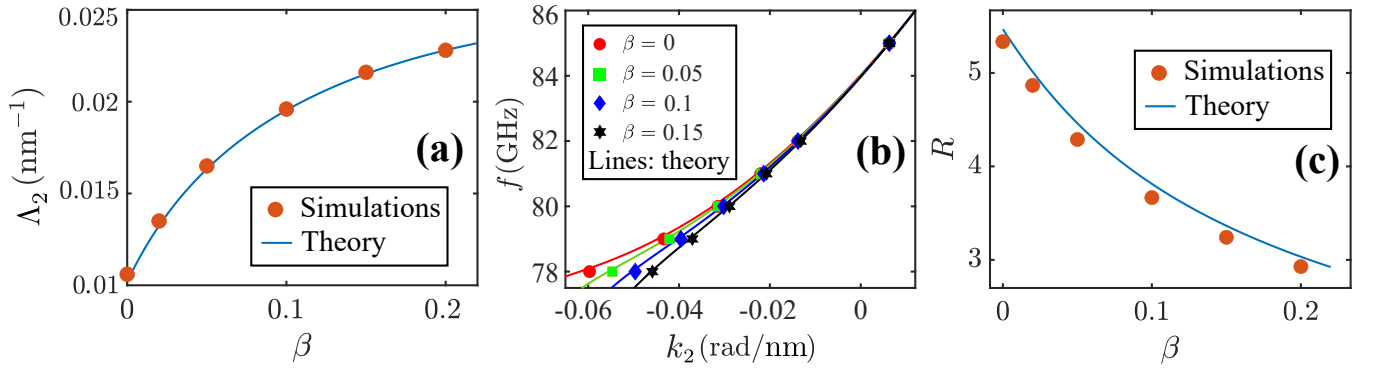


FIG. S3. (a) β -dependence of Λ_2 for spin wave frequency $f = 78$ GHz. (b) Spin wave spectrum ($f - k_2$ relations) for different β . For a given frequency, k_2 increases as β increases. (c) β -dependence of R for $f = 78$ GHz. $\alpha = 0.005$ and various β in the range of $[0, 40\alpha]$ is used throughout the simulations.

6. Simulation results in doped permalloy

In our theory, the frequency window width in which spin waves can be amplified is $f_{\max} - f_{\min} = \frac{1}{2\pi} \frac{u^2}{4A'} = \frac{P^2 \mu_0 \mu_B^2 j^2}{16\pi\gamma e^2 M_s A}$. For material (Co/Pt) parameters used in main text, the required current density for spin wave amplification at useful frequencies is order of 10^{13} A m⁻². One may use point contact structures [S15, S16] to realized such a high current density and corresponding frequency window width is about 6 GHz. Material with lower saturation magnetization M_s and exchange stiffness A , the required current density can be lower. For silver (Ag)-doped permalloy (Py) [S17] with $M_s = 0.39 \sim 0.7$ MA m⁻¹ and $A = 2.8 \sim 11$ pJ m⁻¹, the required current density can be reduced to the order of 10^{12} A m⁻² (See e.g. Ref. [S18] for possible experimental realization) with a frequency window width of 0.5 GHz.

In our simulations showed below, the applied current density is $j = 1.2 \times 10^{12}$ A m⁻² with $P = 1$, $M_s = 0.4$ MA m⁻¹, $A = 3$ pJ m⁻¹, $K_1 = 0.02$ MJ m⁻³, $K_2 = 0.03$ MJ m⁻³, non-adiabatic STT coefficient $\beta = 0.01$, and $\alpha = 0.005$. The frequency of spin wave with zero wave number is 2.8 GHz in current-free region and 4.2 GHz in current-flow region. The frequency window of amplification is $f \in [3.7, 4.2]$ GHz. The simulation procedures are the same as those in Sec. 4. The wave numbers and amplitudes extracted by using Prony method are presented in Fig. S4 (a) and (b). Fig S4 (c) shows clearly supper-reflection $R > 1$ ($T < 0$) in at frequency $f \in [f_{\min}, f_{\max}]$ and $k_2 < 0$.

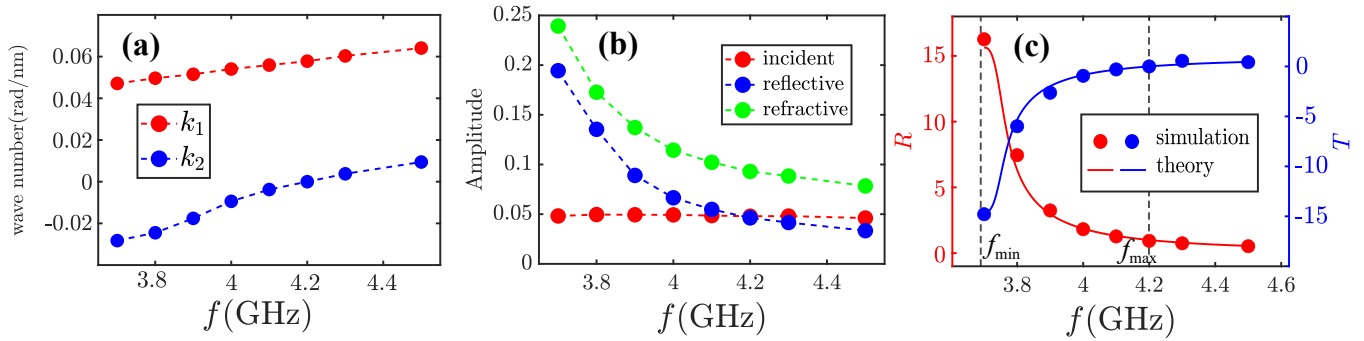


FIG. S4. (a) k_1 -dependence (red dots) and k_2 -dependence (blue dots) of frequency. (b) Amplitudes of the incident wave (red dots), reflective wave (blue dots), and refractive wave (green dots) as functions of frequency. (c) Reflection R and transmission coefficient T versus frequency f . The red and blue solid lines are theoretical predictions of Eq. (5.13). Two dashed lines mark f_{\min} and f_{\max} , respectively.

- [S1] X. S. Wang, Ying Su, and X. R. Wang, Topologically protected unidirectional edge spin waves and beam splitter, *Phys. Rev. B* **95**, 014435 (2017).
- [S2] X. S. Wang, H. W. Zhang, and X. R. Wang, Topological Magnonics: A Paradigm for Spin-Wave Manipulation and Device Design, *Phys. Rev. Applied* **9**, 024029 (2018).
- [S3] Y. Su, X. S. Wang, and X. R. Wang, Magnonic Weyl semimetal and chiral anomaly in pyrochlore ferromagnets, *Phys. Rev. B* **95**, 224403 (2017).
- [S4] Y. Su and X. R. Wang, Chiral anomaly of weyl magnons in stacked honeycomb ferromagnets, *Phys. Rev. B* **96**, 104437 (2017).
- [S5] A. Vansteenkiste, J. Leliaert, M. Dvornik, M. Helsen, F. G. Sanchez, and B. V. Waeyenberge, The design and verification of MuMax3, *AIP Advances* **4**, 107133 (2014).
- [S6] W. F. Brown, Thermal fluctuations of a single-domain particle. *Phys. Rev.* **130**, 1677 (1963).
- [S7] Carriere R, Moses R L. High resolution radar target modeling using a modified Prony estimator. *IEEE Transactions on Antennas and Propagation*, **40**, 1 (1992).
- [S8] L. Thomas, M. Hayashi, X. Jiang, R. Moriya, C. Rettner, and S. S. P. Parkin, Oscillatory dependence of current-driven magnetic domain wall motion on current pulse length, *Nature (London)* **443**, 197 (2006).
- [S9] M. Hayashi, L. Thomas, Y. B. Bazaliy, C. Rettner, R. Moriya, X. Jiang, and S. S. P. Parkin, Influence of current on field-driven domain wall motion in permalloy nanowires from time resolved measurements of anisotropic magnetoresistance *Phys. Rev. Lett.* **96**, 197207 (2006).
- [S10] R. Moriya, L. Thomas, M. Hayashi, Y. B. Bazaliy, C. Rettner, and S. S. P. Parkin, Probing vortex-core dynamics using current-induced resonant excitation of a trapped domain wall, *Nat. Phys.* **4**, 368 (2008)
- [S11] L. Heyne, M. Kläui, D. Backes, T. A. Moore, S. Krzyk, U. Rüdiger, L. J. Heyderman, A. Fraile Rodríguez, F. Nolting, T. O. Mendes, M. Á. Niño, A. Locatelli, K. Kirsch, and R. Mattheis, Relationship between nonadiabaticity and damping in permalloy studied by current induced spin structure transformations, *Phys. Rev. Lett.* **100**, 066603 (2008)
- [S12] Y. Z. Liu, W. T. Hou, X. F. Han, and J.D Zang, Three-Dimensional Dynamics of a Magnetic Hopfion Driven by Spin Transfer Torque, *Phys. Rev. Lett.* **124**, 127204(2020).
- [S13] M. H. Jin, L. Xiong, N. J. Zhou, B. Zheng, and T. J. Zhou, Universality classes of the domain-wall creep motion driven by spin-transfer torques, *Phys. Rev. E*, **103**, 062119(2021).
- [S14] W. W. Wang, P. F. Hu, L. Y. Kong, D. S. Song, and H. F. Du, Magnetic skyrmion Walker breakdown in cylindrical nanotubes, *Phys. Rev. B* **107**, 134407(2023).
- [S15] Excitation of a magnetic multilayer by an electric current M. Tsoi, A. G. M. Jansen, J. Bass, W.-C. Chiang, M. Seck, V. Tsoi, and P. Wyder, *Phys. Rev. Lett.* **80**, 4281 (1998).
- [S16] Y. Ji, C. L. Chien, and M. D. Stiles, Current-induced spin-wave excitations in a single ferromagnetic layer, *Phys. Rev. Lett.* **90**, 106601 (2003).
- [S17] Y. Yin, F. Pan, M. Ahlberg, M. Ranjbar, P. Dürrenfeld, A. Houshang, M. Haidar, L. Bergqvist, Y. Zhai, R. K. Dumas, A. Delin, and J. Åkerman, Tunable permalloy-based films for magnonic devices, *Phys. Rev. B* **92**, 024427 (2015)
- [S18] A. Meo, J. Churemart, R. W. Chantrell, P. Churemart, Magnetisation switching dynamics induced by combination of spin transfer torque and spin orbit torque, *Sci. Rep.* **12**, 3380(2022).